Journal of Catalysis 271 (2010) 43–51

Contents lists available at ScienceDirect

Journal of Catalysis

journal homepage: www.elsevier.com/locate/jcat

Structure, acidity and activity of CuO_x/WO_x–ZrO_2 catalyst for selective catalytic reduction of NO by NH_3

Zhichun Si, Duan Weng *, Xiaodong Wu, Jia Li, Guo Li

State Key Laboratory of New Ceramics & Fine Process, Department of Materials Science and Engineering, Tsinghua University, Beijing 100084, China

ARTICLE INFO

Article history:
Received 9 September 2009
Revised 22 November 2009
Accepted 28 January 2010
Available online 6 March 2010

Keywords:
NH_3-SCR
CuO_x/WO_x–ZrO_2
Low-temperature
Reaction route

ABSTRACT

A series of CuO_x/WO_x–ZrO_2 catalysts were synthesized by impregnating different amounts of copper on the coprecipitated WO_x–ZrO_2 support and were characterized by XRD, BET, XPS, NH_3/NO chemisorption, NH_3-TPO and NH_3-SCR activity measurements. A wide temperature range (200–320 °C) in which NO conversion exceeds 80% is achieved on the 10 wt.% CuO_x/WO_x–ZrO_2 catalyst. The activity and selectivity of the catalysts for ammonia oxidation and NH_3-SCR reaction are determined by the strength and amount of Lewis acid sites and Brønsted acid sites, which are adjusted by the formation of WO_x–ZrO_2 solid solutions and the addition of copper oxides. Two different reaction routes, "ammonia–NO_2 route" at low temperatures (<200 °C) and "amine–NO/NO_2" at high temperatures (>250 °C), are presented for SCR reaction over CuO_x/WO_x–ZrO_2 catalysts.

1. Introduction

Nitrogen oxides (NO, NO_2 and N_2O) emitted from stationary boilers and mobile engines contribute to a lot of environmental problems, for instance, acid rain, photochemical smog, ozone depletion and greenhouse effects [1–3]. With increasingly stringent requirements for fuel economy and vehicle exhaust emission standards, the lean burn engine system has been widely used for fuel economy. Due to the high *A*/*F* ratio used in lean burn conditions, CO and hydrocarbons in exhaust of diesel engines are remarkably decreased compared to those from gasoline engine, which lead to a shortage of reducing agents for three-way catalysis. Therefore, NO_x abatement under oxygen-rich conditions receives much attention. Selective catalytic reduction (SCR) using ammonia [4] or hydrocarbons [5] as reducing agents, and NO_x storage reduction catalysis (NSR) [6] are currently the most favored technologies for purifying NO_x in lean burn engine exhaust [7]. The commercially available technology for reducing NO_x emission from stationary sources is the NH_3-SCR over V_2O_5–WO_3/MoO_3–TiO_2. Commercially available catalysts contain 0.5–3 wt.% V_2O_5, 6–10 wt.% WO_3 (and/or MoO_3) and titania (anatase) support [4,8]. V_2O_5–WO_3/MoO_3–TiO_2 SCR catalysts, which have high NH_3-SCR activity in temperature range of 280–400 °C, have been demonstratively used in the reduction of NO_x from heavy-duty diesel engine with urea as reducing agent. NH_3-SCR catalysts are also investigated for deNO_x of light-duty diesel engine [7]. However, there are still a number of issues concerning improving conversion of NO at low temperatures by developing NH_3-SCR catalysts for light-duty diesel vehicles [7,9–13].

Various catalysts have been investigated for low-temperature NH_3-SCR deNO_x, such as transition metal oxides (CoO_x/CuO_x [13], MnO_x [14,15] and V_2O_5/TiO_2 [16]), zeolite-based catalyst [10,17] and precious metal catalysts [18,19]. Among these catalysts, V_2O_5 is toxic and precious metals are expensive. Transition metal exchanged zeolites (such as Cu-ZSM and Fe-ZSM), which present both attractive NH_3-SCR and HC-SCR activities at low temperatures, have been extensively reported [20–23]. However, their applications are greatly restrained by the poor hydrothermal stability of zeolites. Thus, it is important to develop more stable catalysts such as metal oxides-based SCR catalysts [24].

Copper oxide catalysts on various supports, such as CuO_x/ZrO_2 [25–28], CuO_x/γ-Al_2O_3 [29], CuO_x/SiO_2 [30] and CuO_x/TiO_2 [31,32], show good low-temperature NH_3-SCR activities. The activity and selectivity of copper-based catalysts are determined to a great extent by texture and dispersion state of CuO_x species which are importantly influenced by surface state of supports [25–33]. It has been reviewed that copper oxide supported on zirconia is more active than those on titanium and alumina in the NO + NH_3 reaction, due to a faster NH_3 dissociative chemisorption on the former catalyst [33]. In order to improve the catalytic activity of copper catalyst for NO reduction, more works are required to investigate the relationship between the supports and active sites of catalysts for high NH_3-SCR activity. WO_3 is widely used in V_2O_5–TiO_2 (anatase) modification to improve the dispersion of V_2O_5, thermal stability, surface area, sulfur resistance, NH_3-SCR activity and selectivity of V_2O_5–TiO_2 catalysts [4,34]. WO_3 is also added to zirconia for isomerization and alkylation of hydrocarbons due to the

* Corresponding author. Fax: +86 10 62772726.
E-mail address: duanweng@tsinghua.edu.cn (D. Weng).

0021-9517/$ - see front matter © 2010 Elsevier Inc. All rights reserved.
doi:10.1016/j.jcat.2010.01.025

large surface area and high acid intensity of WO_3–ZrO_2 solid solutions [35–40]. Recently, V_2O_5 supported on WO_3–ZrO_2 solid solutions has been reported in the application of NH_3-SCR [41] and ammonia oxidation [42], which shows high resistance toward alkali poisoning. However, the temperature region for high NH_3-SCR activity of WO_3–ZrO_2-based catalysts is generally located at 350–450 °C, indicating that the low-temperature activity of these catalysts is still need to be improved.

In the present work, we employed a WO_3–ZrO_2 solid solution support (10 wt.% WO_x) instead of pure zirconia in order to improve the low-temperature NH_3-SCR activity of the Cu-containing catalysts and to broaden the temperature window for NO conversion. The effect of the copper loading amount on the activity of the catalyst was studied. By means of *in situ* FTIR tests of NH_3, NO and NH_3 + NO + O_2 adsorption, the effects of WO_x modification on the surface properties of catalysts and mechanisms of NH_3-SCR reaction over CuO_x/WO_x-ZrO_2 at various temperatures were explored.

2. Experimental

2.1. Catalysts preparation

WO_x-ZrO_2 solid solutions were synthesized by coprecipitation method. $ZrO(NO_3)_2{\cdot}5H_2O$ (AR grade, 99%, Rongruida) and $5(NH_4)_2O{\cdot}12WO_3{\cdot}5H_2O$ (AR grade, 99%, Tianjin Juneng) with the weight ratio of W:Zr = 1:9 were dissolved in deionized water by magnetic stirring. Excess ammonia was added to keep the pH value of the mixed solution at 10. The obtained mixture was dried at 100 °C for 4 h. Then, the precipitates were dried at 110 °C overnight and calcined at 500 °C for 3 h in static air in a muffle to obtain the WO_x–ZrO_2 solid solution powders. ZrO_2 was prepared by the similar method.

CuO_x/WO_x–ZrO_2 catalysts were prepared by wet incipient impregnation method. Water absorption capacity of WO_x–ZrO_2 powders was measured as 23 wt.%. The copper nitrate was dissolved in the maximal amount of water absorbable by the support and then mixed with WO_x–ZrO_2 powders. The mixture was dried at 100 °C for 4 h and calcined at 500 °C for 1 h in static air in a muffle to obtain CuO_x/WO_x–ZrO_2 catalysts with the compositions listed in Table 1. The nominal weight ratios of copper oxide loaded and the tungsten oxide in the WO_x–ZrO_2 support were calculated in terms of CuO and WO_3, respectively.

2.2. Characterizations

The powder X-ray diffraction (XRD) experiments were performed on a Japan science D/mas-RB diffractometer employing Cu Kα radiation (λ = 0.15418 nm). The X-ray tube was operated at 40 kV and 120 mA. The X-ray powder diffractogram was recorded at 0.02° intervals in range of 20° < 2θ < 80°. The identification of the phases was made with the help of JCPDS cards (Joint Committee on Powder Diffraction Standards). The mean crystallite sizes of tetragonal zirconia and CuO were calculated by Scherer formula.

The specific surface areas of the samples were measured using the N_2 physisorption at −196 °C by Brunauer–Emmett–Teller (BET) method using an automatic surface analyzer (Quantachrome NOVA instrument). The samples were degassed in flowing N_2 at 200 °C for 2 h.

Table 1
Compositions of the catalysts.

Sample	CuO_x (wt.%)	WO_x (wt.%)	ZrO_2 (wt.%)
$W10ZrO_2$	–	10	90
$Cu5W10ZrO_2$	5	9.5	85.5
$Cu10W10ZrO_2$	10	9	81
$Cu20W10ZrO_2$	20	8	72
$Cu10ZrO_2$	10	–	90

The X-ray photoelectron spectroscopy (XPS) experiments were carried out on a PHI-Quantera SXM system equipped with a monochromatic Al Kα X-rays under UHV (6.7×10^{-8} Pa). Sample charging during the measurement was compensated by an electron flood gun. The electron takeoff angle was 45° with respect to the sample surface. The XPS data from the regions related to the Cu 2*p* and W 4*f* core levels were recorded for each sample. The binding energy was calibrated internally by the carbon deposit C 1*s* binding energy (BE) at 284.8 eV.

In situ FTIR spectra of adsorption species arising from NO or NH_3 chemisorption were recorded in the range of 4000–650 cm^{-1} using a thermo Nicolet 6700 FTIR spectrometer equipped with a high-temperature environmental cell fitted with KBr window. Prior to reactant gas (NH_3 or NO) chemisorption, the sample was placed in a crucible located in the high-temperature cell and heated up to 500 °C in a 20% (v/v) O_2/N_2 flow (100 ml min^{-1}). After the oxidation treatment at 500 °C for 30 min, the samples were cooled down to the corresponding temperature, and subsequently, flushed by 100 ml min^{-1} N_2 for 30 min to remove the physisorbed molecules for background collection. Then, the gas mixture contained 1000 ppm NO + 1% O_2 or NH_3 + 1% O_2 in N_2 (100 ml min^{-1}) was passed through the sample at the corresponding temperature for 30 min. The FTIR spectra were collected after purging the weak adsorbed gas molecules by N_2 flow gases for 30 min.

In situ FTIR spectra of adsorption species arising from NO, NH_3 and O_2 co-adsorption on catalysts, which were operated in the similar conditions of NO chemisorption, were collected after co-adsorption by 1000 ppm NO and 1000 ppm NH_3 in 1% O_2 + N_2.

2.3. Activity measurement

The catalytic activity measurement for the reduction of NO by ammonia (NH_3-SCR) with excess oxygen was carried out in a fixed bed reactor made of stainless steel with 0.5 g catalysts (diluted to 2 ml by silica) inside. The reaction gas mixture simulating diesel engine exhaust gases consisted of 500 ppm NO, 500 ppm NH_3, 5% O_2 and N_2 in balance. The NO conversion was measured from room temperature to 500 °C at a heating rate of 10 °C min^{-1}. The total flow of the gas mixture was 1 L min^{-1} at a gas hourly space velocity (GHSV) of 30,000 h^{-1}. The concentrations of nitrogen oxides and ammonia were measured at 120 °C by a Thermo Nicolet 380 FTIR spectrometer equipped with 2 m path length sample cell (250 ml volume). Gas path from the reactor to FTIR spectrometer was maintained a constant temperature at 120 °C to avoid NH_4NO_2/NH_4NO_3 deposition.

The NO/NH_3 conversions were calculated as follows:

$$NO/NH_3 \text{ conversion } (\%) = \frac{C_{in} - C_{out}}{C_{in}} \times 100 \quad (1)$$

where C_{in} and C_{out} denoted the inlet and outlet gas concentration of NO (or NH_3), respectively.

Ammonia temperature-programmed oxidation (NH_3-TPO) tests were carried out using a similar method to NH_3-SCR experiment with 500 ppm NH_3 and 5% O_2 in N_2. Onset temperatures of ammonia and NO conversions were defined as the temperature when ammonia and NO conversions exceeded 4%. The temperature window for SCR reaction was defined as the temperature region in which NO conversion exceeded 80%.

3. Results

3.1. Activity studies

3.1.1. Activity for NH_3 oxidation

NH_3-TPO experiments were carried out to test the ammonia oxidation activity of catalysts. Fig. 1a shows the ammonia conver-

sion as a function of temperature during NH_3-TPO process over various catalysts. $W10ZrO_2$ catalyst, on which the onset temperature of ammonia oxidation is 300 °C, presents a much lower ammonia oxidation activity than $Cu10ZrO_2$ catalyst. This demonstrates the role of copper oxides as the main active sites for ammonia oxidation. It is also confirmed by the order of onset temperature on CuO_x/WO_x–ZrO_2 catalysts as a function of CuO_x loading amount: the higher the CuO_x loading amount, the lower the onset temperature of ammonia oxidation. On the other hand, given the same loading amount of CuO_x (10 wt.%), the onset temperature of ammonia conversion on $Cu10W10ZrO_2$ (215 °C) shifts to higher temperature by 15 °C compared to that on $Cu10ZrO_2$ (200 °C). It implies the inhibition effect of WO_x on ammonia oxidation over the catalyst.

The evolution of NO_x (NO, NO_2 and N_2O) generated during NH_3-TPO process is shown in Fig. 1b–d, respectively. On all catalysts, containing WO_3 or not, increasing temperature causes the NO_x products to increase monotonically. However, the productions of NO_x are obviously inhibited by the WO_x–ZrO_2 solid solution support. On the other hand, the higher the copper loading amount, the lower temperature at which NO_x start to generate, and the higher amount of NO_x is produced. The production of N_2 was not detected due to the limitation of laboratory instruments. However, the delay between ammonia conversion and NO_x evolutions can be considered to arise from ammonia oxidation to N_2 at low temperatures [43,44]. With increasing the temperature, the oxidation of ammonia to NO_x becomes the dominant reaction.

3.1.2. Activities for NH_3-SCR

NH_3-SCR performances of various catalysts were measured as a function of temperature, and the results are shown in Fig. 2a. For $W10ZrO_2$ catalyst, NO conversion starts at 250 °C and exceeds 77% at 380–480 °C. The onset temperature of NH_3-SCR reaction decreases down to 150 °C for $Cu5W10ZrO_2$ and about 125 °C for those catalysts with higher CuO_x content. Thus, copper oxide plays an important role in low-temperature NH_3-SCR reaction. Among these catalysts, $Cu10W10ZrO_2$ shows the highest low-temperature NH_3-SCR activity. Comparatively, the maximal NO conversion on $Cu10ZrO_2$ only reaches 70%, indicating that WO_x addition can remarkably enhance the NH_3-SCR activity of CuO_x/ZrO_2 catalysts and broaden the temperature window for NO conversion.

Fig. 2b shows the NH_3 conversion as a function of temperature over various catalysts during NH_3-SCR reaction. Ammonia conversion on CuO_x-containing catalysts all start around 120 °C and reach 100% in the temperature range of 220–250 °C. However, ammonia conversion over $W10ZrO_2$ does not start until 280 °C or reach a maximum even at 500 °C. It is clear by comparison between Figs. 2b and 1a that the onset temperatures of ammonia conversion over

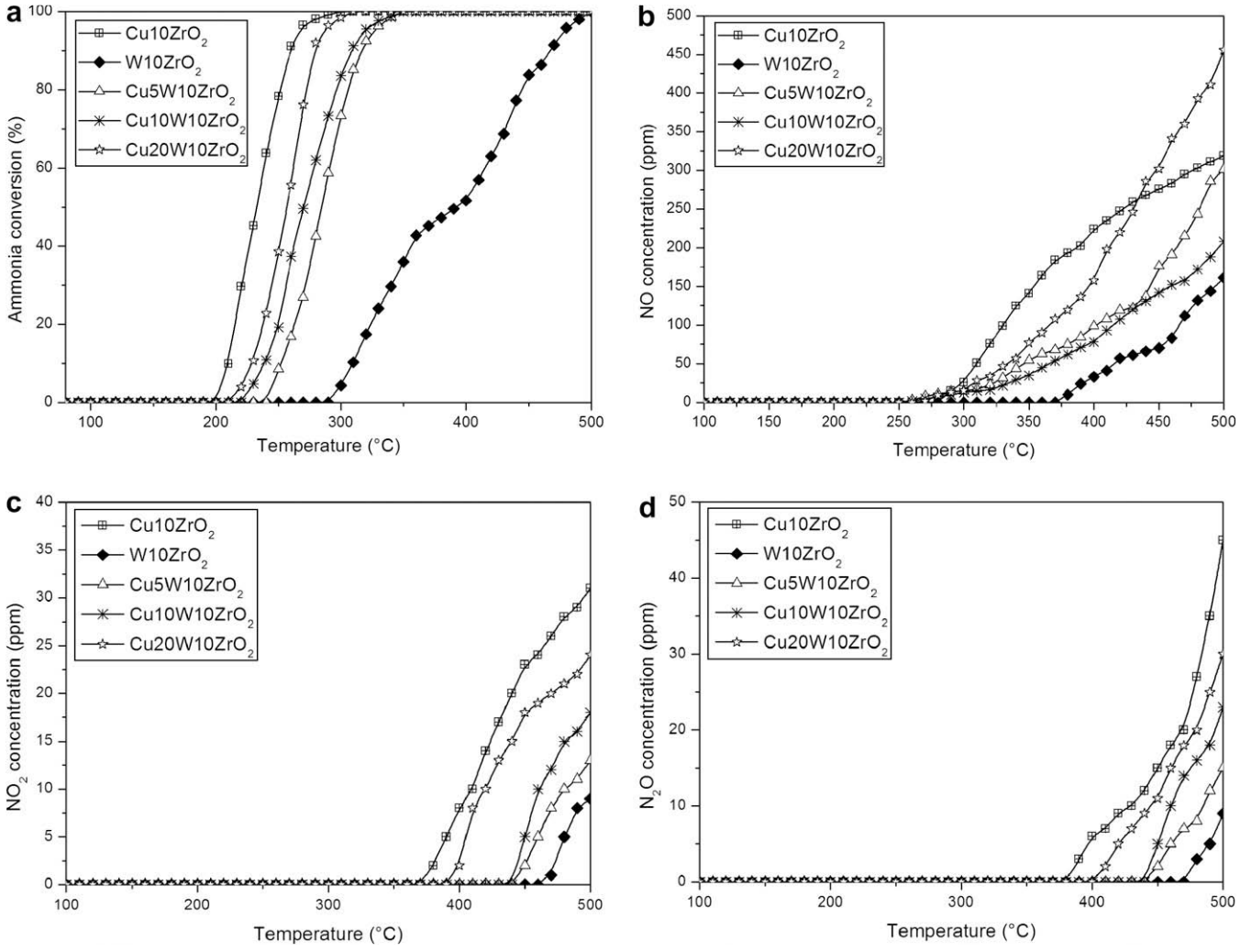

Fig. 1. (a) NH_3 conversion as a function of temperature over various catalysts during NH_3-TPO process. (b) NO generation as a function of temperature over various catalysts during NH_3-TPO process. (c) NO_2 generation as a function of temperature over various catalysts during NH_3-TPO process. (d) N_2O generation as a function of temperature over various catalysts during NH_3-TPO process.

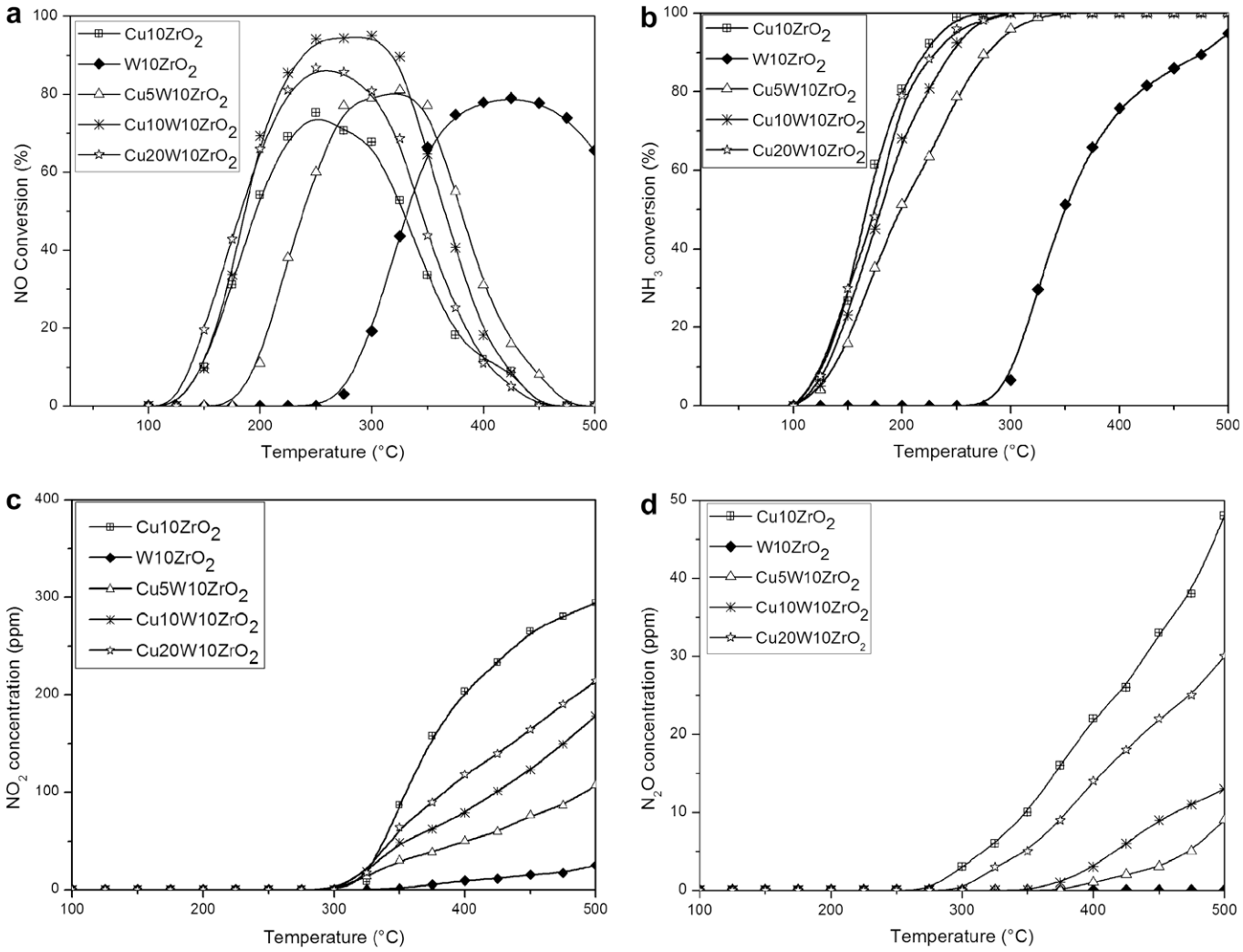

Fig. 2. (a) NO conversion as a function of temperature on various catalysts during NH_3-SCR process. (b) NH_3 conversion as a function of temperature on various catalysts during NH_3-SCR process. (c) NO_2 generation as a function of temperature on various catalysts during NH_3-SCR process. (d) N_2O generation as a function of temperature on various catalysts during NH_3-SCR process.

CuO_x-containing catalysts in SCR reaction (120 °C) are much lower than those in NH_3-TPO tests (above 200 °C). Furthermore, if we compare Fig. 2b with Fig. 2a, NH_3 conversion is found to follow the trend of NO conversion initially but exceed the latter at temperatures higher than 250 °C. It implies that ammonia prefers to reacting with NO_x-derived species (such as nitro compounds) rather than O_2 at low temperatures, and the latter becomes the dominant oxidizing agent for ammonia oxidation at high temperatures. Thus, it is assumed that the NH_3-SCR reaction may follow different mechanisms at various temperature ranges (<200 °C and >250 °C).

The evolution of NO_2 during NH_3-SCR reaction is shown in Fig. 2c. NO_2 forms at 300 °C at which ammonia conversion reaches 100%, which is lower than the onset temperature of NO_2 generation in NH_3-TPO process (370 °C in Fig. 1c). This fact indicates that the NO_2 originates from NO oxidation with the consumption of ammonia in NH_3-SCR reaction. The NO_2 production increases with increasing the CuO_x content in catalysts, which is ascribed to the strong activity of copper species for NO oxidation.

The outlet N_2O concentration during NH_3-SCR reaction was also recorded, and the results are shown in Fig. 2d. N_2O is not observed over $W10ZrO_2$ during the whole testing process, but appears at temperatures above 200 °C on those CuO_x-containing catalysts. Similar as the generation of NO_2, the N_2O production also increases as a function of the CuO_x loading amount. Busca et al. [4] have reviewed that nitrous oxide generation is mainly related to ammonia oxidation at high temperatures and ammonia nitrate formation at relative lower temperatures over low-temperature catalysts. This point of view is confirmed in our work that the onset temperatures of N_2O generation in NH_3-SCR process are much lower than those in NH_3-TPO reactions. Much less N_2O is produced on $Cu10W10ZrO_2$ than on $Cu10ZrO_2$, indicating the inhibition effect of WO_x modification on the N_2O generation due to the restrained formation of nitrates on the surface of tungsten-containing catalysts. N_2O production increases with the increase in copper content both in NH_3-TPO and NH_3-SCR process, indicating that ammonia oxidation may account for the N_2O generation at relative high temperatures.

3.2. BET and XRD studies

The presence of zirconia, copper oxides and tungsten oxides crystallites was ascertained by XRD, and the diffraction patterns of all samples are shown in Fig. 3. The characteristic peaks of both tetragonal-ZrO_2 (t-ZrO_2) and monoclinic-ZrO_2 (m-ZrO_2) are observed in the diffraction pattern of tungsten-free $Cu10ZrO_2$, while only those of t-ZrO_2 appear on the tungsten-containing samples.

It agrees with the previous reports that transformation of the *t*-ZrO_2 phase to the more thermodynamically stable *m*-ZrO_2 phase can be restrained by the addition of transition metals [37,38]. No characteristic peaks of WO_x are found for all samples, indicating the formation of WO_x–ZrO_2 solid solutions [37,38]. According to smaller ionic radii of W^{6+} (0.65 Å) and W^{5+} (0.66 Å) than that of Zr^{4+} ions (0.79 Å), W^{6+} and W^{5+} ions may be incorporated into the zirconia lattice to form WO_x–ZrO_2 solid solutions and stabilize the *t*-ZrO_2 [37]. Compared to $Cu10ZrO_2$, the intensity of CuO (1 1 1) diffraction peak at $2\theta = 38.6°$ is obviously decreased on Cu10W10Z-rO_2, which suggests the better dispersion of CuO_x on WO_x–ZrO_2 solid solutions than on zirconia. The intensity of CuO peaks increases as a function of the loading amount due to the crystallization and sintering of CuO_x on the surface of WO_x–ZrO_2.

The BET surface areas, crystal size of CuO and ZrO_2 of the catalysts, are summarized in Table 2. The specific surface area of the catalyst decreases with the increase in the CuO_x content, which may be caused by blocking effect of the support pores by the loading of metal oxide. Smaller crystallite sizes of CuO on WO_x–ZrO_2 indicate the higher dispersion of copper oxide on WO_x–ZrO_2 than on ZrO_2.

3.3. XPS studies

In order to obtain the information of oxidation state of copper cations on the catalyst surface, XPS spectra of the samples was detected. The Cu 2*p* spectra of the CuO_x-containing samples are shown in Fig. 4a. The fittings of Cu 2*p* peaks were performed by two components, which present BE at 933.9 and 932.9 eV corresponding to surface Cu^{2+} and Cu^{+}/Cu^{0} species, respectively. It has been well established that the presence and absence of the shake-up peak centered at 944 eV are indicators of Cu^{2+} species and lower valence copper species (Cu^{+}/Cu^{0}) [24,26]. The relative percentages of copper species were calculated by the area ratio of the corresponding characteristic peaks. The results are listed in Table 3. In comparison with the $Cu10ZrO_2$ catalyst, more Cu^{2+} are reduced to low-valence copper species on the surface of the WO_x–ZrO_2 support, which may be ascribed to the well dispersion of CuO_x on WO_x–ZrO_2 and strong interaction between metal and support. With increasing the loading amount of CuO_x, the sintering of CuO clusters leads to an increase in the $Cu^{2+}/(Cu^{+}/Cu^{0})$ ratio.

The W 4*f* spectra of the tungsten-containing samples are shown in Fig. 4b. The W $4f_{7/2}$ BE values are located at 35.8 ± 0.2 and 34.8 ± 0.2 eV, corresponding to characteristic of W^{6+} and W^{5+}, respectively [37]. The W^{6+}/W^{5+} ratios calculated by the area ratios of corresponding peaks are shown in Table 3. In comparison with pure WO_x–ZrO_2 solid solutions, the loading of copper oxide leads to a partial reduction of W^{6+} to W^{5+}. Again, this fact suggests some strong interaction between copper and tungsten which will be demonstrated in further work.

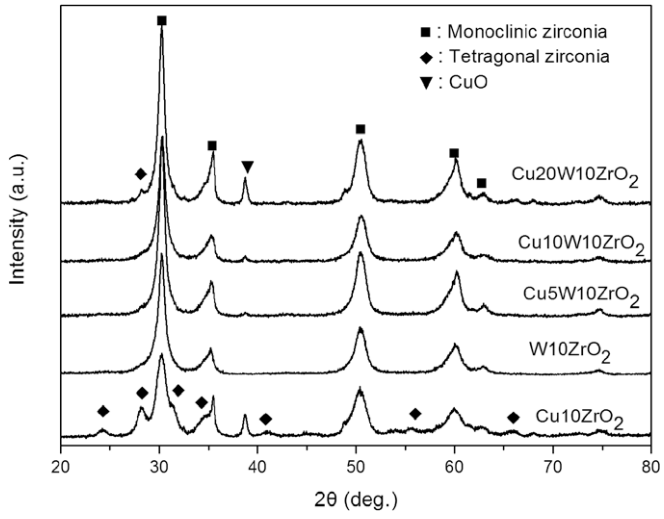

Fig. 3. XRD patterns of the catalysts.

3.4. NH_3 chemisorptions

FTIR spectra of adsorbed species on surface of catalysts arising from ammonia adsorption at room temperature are shown in Fig. 5a. All spectra show sharp bands in the region of 1615–1600 cm^{-1} and 1220–1200 cm^{-1}, corresponding to σ_{as} and σ_s model of NH_3 coordinated to Lewis acid sites, respectively. The band at 1600 cm^{-1} in the spectrum of $W10ZrO_2$ shifts to 1615 cm^{-1} after loading CuO_x, indicating the increased Lewis acidity of CuO_x/WO_x–ZrO_2. Sharp bands at 1680 and 1470 cm^{-1} are found only in the spectrum of WO_x/ZrO_2, which are attributed to σ_s NH_4^+ and σ_{as} NH_4^+ resulting from ammonia coordinated to Brønsted acid sites. By loading CuO_x, the concentration of Brønsted acid sites decreases according to the obviously weakened band at 1470 cm^{-1} on $Cu5W10ZrO_2$, $Cu10W10ZrO_2$ and $Cu20W10ZrO_2$. The concentrations of Lewis and Brønsted acid sites on catalysts were determined by the area of the absorption bands corresponding to the σ_s NH_3 and σ_{as} NH_4^+ models, respectively [32]. High concentrations of Lewis acidity are obtained on tungsten-containing catalysts with intense and broad adsorption bands at 1213 cm^{-1}. Moreover, the band shape seems to be regardless of the loading amount of copper oxide, implying the preferential adsorption of NH_3 on WO_x–ZrO_2 solid solutions. This may reduce the ammonia inhibition effect, which is usually caused by competitive adsorptions of NH_3 and NO on Cu^{n+} active sites [45] and will be discussed later. In comparison with $W10ZrO_2$, the weak bands at 1680 and 1470 cm^{-1} in spectra of CuO_x/WO_x–ZrO_2 catalysts indicate the negative effect of CuO_x on Brønsted acidity.

Fig. 5b shows the FTIR spectra of adsorbed species on surface of catalysts arising from ammonia adsorption at 200 °C. In comparison with the spectra obtained at room temperature, ammonia adsorption at 200 °C yields complex bands in the region of 1500–1290 cm^{-1} and a new band at 1710 cm^{-1}, which are ascribed to ammonia oxidation intermediates and Brønsted bonded NH_4^+ [32]. Bands corresponding to σ_s model of NH_3 become sharpened and shift from 1213 to 1240–1220 cm^{-1}, indicating that ammonia bonded to Lewis acid sites are more stable. Intensity of the band at 1615–1600 cm^{-1} greatly decreases due to desorption of ammonia at high temperatures. The diminishing of adsorption bands on $Cu10ZrO_2$ indicates that ammonia species adsorbed on the tungsten-free catalyst are less stable.

3.5. NO chemisorptions

FTIR spectra of adsorbed species on surface of catalysts arising from NO adsorption at room temperature are shown in Fig. 6a. According to the literature [25], NO adsorption on Cu–ZrO_2/SO_4^{2-} yields an intense band at 1900 cm^{-1} and a weak band at

Table 2
Textural and structural properties of the catalysts.

Samples	BET surface area ($m^2\ g^{-1}$)	Crystallite size of CuO (nm)	Crystallite size of *t*-ZrO_2 (nm)
$Cu10ZrO_2$	19.0	12.7	14.4
$W10ZrO_2$	99.3	–	7.0
$Cu5W10ZrO_2$	74.0	4.3	8.6
$Cu10W10ZrO_2$	70.0	5.5	8.6
$Cu20W10ZrO_2$	50.0	8.7	10.5

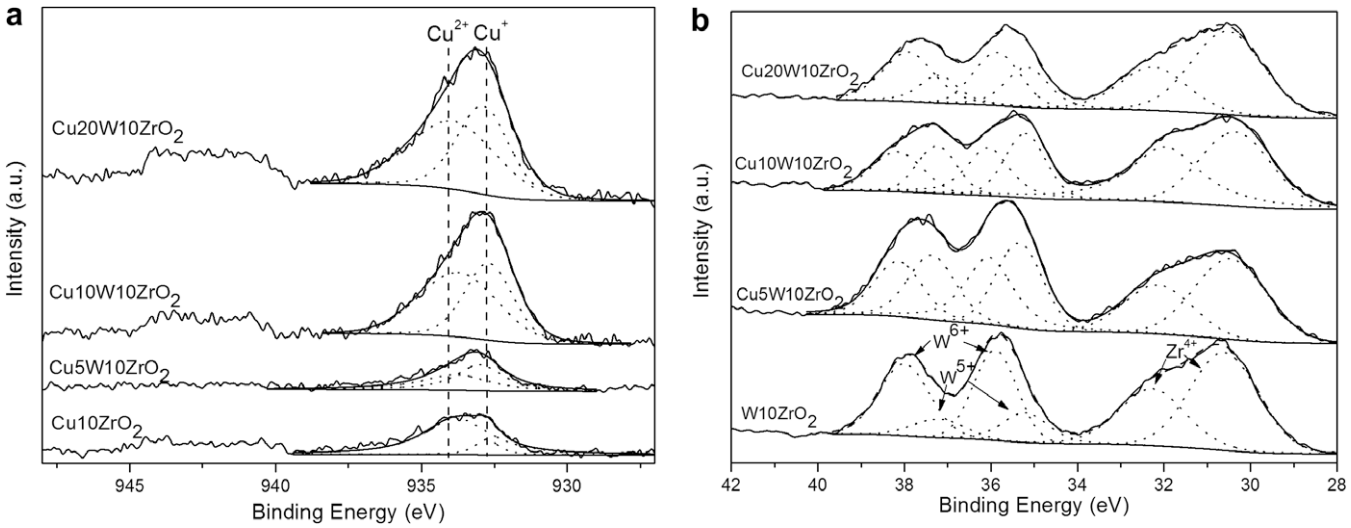

Fig. 4. XPS spectra of catalysts: (a) Cu 2*p* and (b) W 4*f*.

Table 3
Different oxidation states of surface Cu (2*p*) and W (4*f*) measured by XPS.

Samples	Cu^{2+}/Cu^{+}	W^{6+}/W^{5+}
$Cu10ZrO_2$	6.6	–
$W10ZrO_2$	–	2.5
$Cu5W10ZrO_2$	1.2	1.3
$Cu10W10ZrO_2$	1.3	1.0
$Cu20W10ZrO_2$	1.9	0.9

1810 cm^{-1} corresponding to Cu^{2+}–NO and Cu^{+}–NO, respectively. In this case, the band at 1885 cm^{-1} on CuO_x/WO_x–ZrO_2 catalysts can be assigned to Cu^{2+}–NO. It is known that Cu^{+} ions can be oxidized to Cu^{2+} in the presence of NO, which may explain the absence of Cu^{+}–NO species [24,28]. Band assigned to Cu^{2+}–NO species disappears in the spectrum of $Cu10ZrO_2$, implying rapid desorption of NO from the catalyst. The spectrum of $W10ZrO_2$ shows two broad bands at 2112 and 1935 cm^{-1}, assigned to the first overtone of W = O stretching modes (with another band at about 980 cm^{-1} ascribed to W = O symmetrical stretching mode) and W^{n+}–NO, respectively. With increasing the CuO_x loading amount, the absorption band in the region of 2200–2000 cm^{-1} disappears and the band at 980 cm^{-1} decreases sharply, which are probably caused by coverage of WO_x by CuO_x. It is seen by the variation in intensity of band at 1885 cm^{-1} that the Cu^{2+}–NO bond is more stable on highly dispersed CuO_x species. From the weak bands at 1615–1600 cm^{-1} for the CuO_x-supported catalysts, nitrate formation on WO_x–ZrO_2 is inhibited by CuO_x loading. Instead, nitro compounds (1500–1450 cm^{-1}) are more easily formed on these catalysts.

The NO adsorption test was also performed at 200 °C, and the FTIR spectra are shown in Fig. 6b. Band at 1900–1850 cm^{-1} disappears due to the instability of metal mononitrosyls at this temperature. Band at 1600 cm^{-1} in the spectrum of $W10ZrO_2$ splits into bimodal bands at 1622 and 1568 cm^{-1}, which are assigned to υ_3 models of bridging and bidentate nitrates, respectively [40]. Multi-bands in the regions of 1500–1360 and 1350–1200 cm^{-1} ascribed to the surface nitro compounds are observed for all samples. The negative bands at 1650–1550 cm^{-1} implies the easy desorption of surface nitrates from the CuO_x-containing catalysts. Bands at 1002 cm^{-1} in the spectra of tungsten-containing catalysts

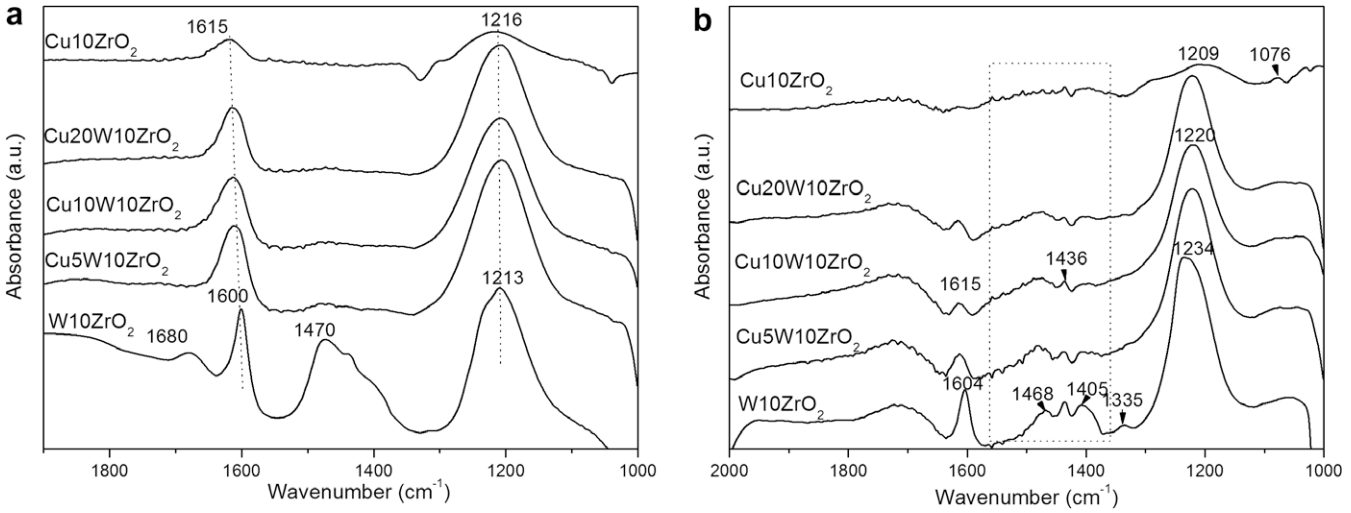

Fig. 5. FTIR spectra of the adsorbed species on surface of catalysts arising from ammonia adsorption: (a) at room temperature and (b) at 200 °C.

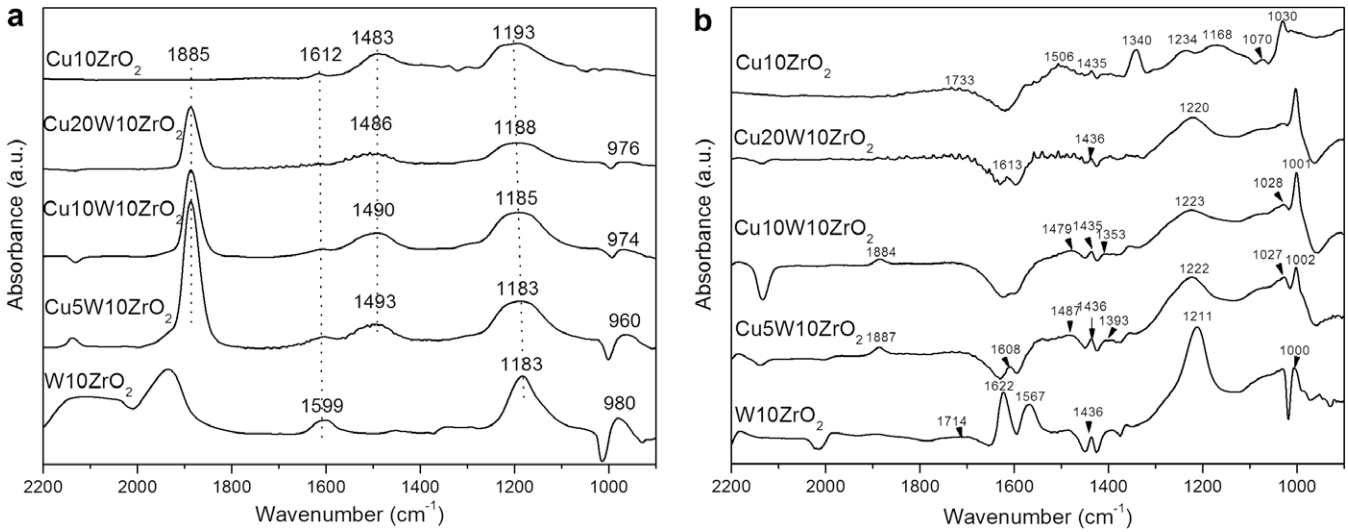

Fig. 6. FTIR spectra of the adsorbed species on surface of catalysts arising from NO adsorption: (a) at room temperature and (b) at 200 °C.

may be ascribed to W = O species [36]. There is no obvious difference between the spectra obtained at 250 °C (not shown) and those collected at 200 °C.

3.6. NH_3, NO and O_2 co-adsorption

In order to investigate possible reactions among the reactants, NH_3, NO and O_2 co-adsorption measurements at various temperatures were carried out on $W10ZrO_2$, $Cu10ZrO_2$ and $Cu10W10ZrO_2$ catalysts. The infrared spectra obtained at 200 °C are shown in Fig. 7a. Bands at 1710 and 1430 cm^{-1} correspond to σ_s and σ_{as} of NH_4^+ adsorbed on Brønsted acid sites, respectively. Asymmetric band at 1500–1400 cm^{-1} may be caused by overlapping of bands of NH_4^+ and nitro compounds [10]. In comparison with the spectra obtained in NH_3 chemisorptions, the enhanced Brønsted acidic surface of $Cu10W10ZrO_2$ may result from the contact of water (generated in NH_3-SCR process) and W = O on surface of catalysts [46]. The small band at 1888 cm^{-1} in the spectrum of $Cu10W10ZrO_2$ is ascribed to NO adsorbed on Cu^{n+} species. The absence of absorption bands (1600–1550 cm^{-1}) indicates that nitrate formation is inhibited to a large extent compared to the case of NO chemisorption (Fig. 6), which may be caused by the competitive adsorption and followed reactions among NH_3, NO and O_2. No absorption bands of NH_4^+ are observed in the spectrum of $Cu10ZrO_2$. The overlapping of σ_s NH_3 and υ_1 modes of nitrite induces a broad band at 1300–1050 cm^{-1} for $Cu10ZrO_2$. Bands at 1613–1604 and 1240–1200 cm^{-1} can be ascribed to ammonia adsorbed on Lewis acid sites. The band at 1215 cm^{-1} indicates the formation of chelating nitro compounds on the surface of $W10ZrO_2$ [45].

FTIR spectra arising from NH_3, NO and O_2 co-adsorption at 250 °C are shown in Fig. 7b. New intense bands appear in the region of 1580–1540 cm^{-1}, indicating the formation of large amounts of amine or hydrazine at 250 °C [32]. Adsorption of NH_3 on Lewis acid sites at 1260–1255 cm^{-1} is greatly reduced, while the bands at 1710–1670 and 1442–1419 cm^{-1} related to ammonia coordinated on Brønsted acid sites (NH_4^+) increase significantly, indicating less stability of NH_3 on Lewis acid sites. The absence of the latter bands in the spectrum of $Cu10ZrO_2$ implies that Brønsted acid sites derive mainly from interaction between H_2O produced by SCR reaction and WO_x–ZrO_2 solid solutions. The bands in the regions of 1500–1300 and 1300–1200 cm^{-1}, together with weaker bands at 1100–1000 cm^{-1}, are ascribed to surface nitro

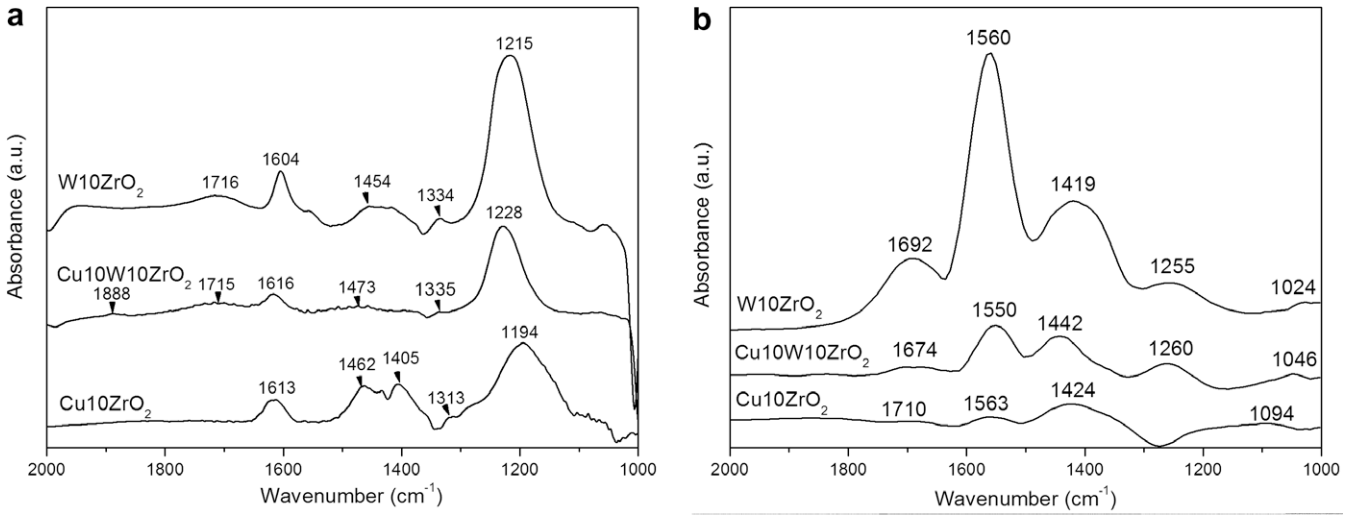

Fig. 7. FTIR spectra of the adsorbed species on surface of catalysts arising from NH_3, NO and O_2 co-adsorption: (a) at 200 °C and (b) at 250 °C.

compounds [28]. The broad negative band at 1280 cm^{-1} in the spectrum of $Cu10ZrO_2$ is caused by the desorption of nitro compounds.

4. Discussion

According to the above results, the difference in the onset temperatures of various gases in NH_3-TPO and NH_3-SCR tests reveals the importance of NO_2 formation for NH_3-SCR reaction at low temperatures, which depends on the copper loading amount of catalysts. However, the temperature window of catalysts for NH_3-SCR does not depend on the copper loading amount alone, and the activity of the tungsten-free catalyst is seriously deactivated at high temperatures. The variation of acid properties on catalysts introduced by copper addition and tungsten modification is suggested to be responsible for the above phenomena. The following discussion is focused on the correlations between acid properties and NH_3-SCR performances of the catalysts.

Based on the models reported [24–29], possible reaction routes for ammonia oxidation and NH_3-SCR processes are presented in Eqs. (2)–(16), respectively. In these reactions, Lewis acid sites and Brønsted acid sites play different roles at various temperatures [4]. Ammonia adsorption experiment shows that no Brønsted acidity was observed on the surface of $Cu10ZrO_2$. However, this catalyst presents ultra high activity in NH_3-TPO reaction, indicating that Brønsted acidity is not necessary for ammonia oxidation. Lewis acid sites on CuO_x/WO_x–ZrO_2 catalysts may arise from the unsaturated coordination of Cu^{n+} and W^{n+} ions. The redox properties of Lewis acidic transition metal oxides are related with reducibility of transition metal ions (M^{n+}). From the XPS results, copper species with lowered valence are generated on catalyst due to tungsten modification. Therefore, the ammonia oxidation activity of catalysts is decreased because of the lowered oxidation activity of copper species (NH_3-TPO results)

$$NH_3(g) + L^*(\text{Lewis acid site}) \rightarrow NH_3(ads) \quad (2)$$

$$NH_3(g) + B^*(\text{Br}\varnothing\text{nsted acid site}) \rightarrow NH_4^+(ads) \quad (3)$$

$$NH_3(ads) \rightarrow NH_2(ads) + H^+ + e^- \quad (4)$$

$$NH_4^+(ads) \rightarrow NH_2(ads) + 2H^+ + e^- \quad (5)$$

$$2NH_2(ads) \leftrightarrow N_2H_4(ads) \quad (6)$$

$$N_2H_4(ads) + O(ads) \rightarrow N_2 + 2H_2O \quad (7)$$

$$2NH_2(ads) + O(ads) \rightarrow 2NH(ads) + H_2O \quad (8)$$

$$NH(ads) + O(ads) \rightarrow HNO(ads) \quad (9)$$

$$2HNO(ads) + O(ads) \rightarrow H_2O + 2NO \quad (10)$$

The reduction of NO to N_2 by NH_3 in excess O_2 is suggested to follow different routes at various temperatures. At low temperatures (<200 °C), the possible reaction steps are:

$$NO + O(ads) \rightarrow NO_2(ads) \quad (11)$$

$$2NH_3(ads) + NO_2(ads) + NO \rightarrow 2N_2 + 3H_2O \quad (12)$$

While at high temperatures (>250 °C), the possible reaction steps are:

$$NH_2(ads) + NO(gas) \rightarrow NH_2NO(ads) \quad (13)$$

$$NH_2NO(ads) \rightarrow N_2 + H_2O \quad (14)$$

$$NH_2(ads) + NO_2(ads) \rightarrow NH_2NO_2(ads) \quad (15)$$

$$NH_2NO_2(ads) \rightarrow N_2 + H_2O + O(ads) \quad (16)$$

According to high low-temperature SCR activities of all the CuO_x-containing catalysts, Lewis acid sites should serve as important active sites at temperatures lower than 200 °C. Since nitro compounds and ammonia coordinated to Lewis acid sites are observed as the dominant species on CuO_x/WO_x–ZrO_2 at 200 °C, it is reasonable to assume that these species are main intermediates in low-temperature NH_3-SCR reaction. In this way, NH_3-SCR process follows Eqs. (11) and (12). NO is supposed to be firstly oxidized and then reduced by ammonia. The corresponding reaction mechanism is defined as "ammonia-NO_2 route", in which both ammonia adsorption on WO_x–ZrO_2 solid solutions (results in NH_3 chemisorptions) and NO oxidation to nitro compounds on copper oxides are essential (results in NO chemisorptions). The active sites are regenerated by the consumption of NO_2^- and adsorbed ammonia with oxygen. Without loading copper oxide, the accumulation of surface nitrites and nitrates on WO_x–ZrO_2 solid solutions results in difficulties for the desorption of nitro compounds and consequently non-low-temperature SCR activity of $W10ZrO_2$, which is called as "NO_x inhibition effect" in the previous literature [47]. After loading copper oxide, nitro compounds are easier to desorb due to quick adsorption/desorption of NO/NO_2 on copper species. In turn, ammonia is preferentially adsorbed on WO_x–ZrO_2 solid solutions, which helps to avoid the ammonia inhibition effect on NO adsorption on copper active sites.

Ammonia-derived species such as NH_2 (Eq. (2)–(6)) become main surface intermediates for SCR reaction at 250 °C, which agrees with the previous reports [25,32]. Thus, "amine-NO/NO_2 route" as Eqs. (13)–(16) become another important NH_3-SCR reaction pathways at high temperatures. Both NO and its oxidation product NO_2 react with amine to form nitrite and nitrate which then decompose to nitrogen. Since both Lewis acid sites and Brønsted acid sites can promote the formation of amine, the increased concentrations of two types of acid sites are responsible for the enhanced activity of CuO_x/WO_x–ZrO_2 with respect to $Cu10ZrO_2$. However, Lewis acid sites are also active for ammonia oxidation to N_2 or nitrogen oxides (Eqs. (6)–(10)), resulting in a decrease in high-temperature NH_3-SCR activity. WO_x–ZrO_2 solid solution can generate considerable Brønsted acid sites during NH_3-SCR process as confirmed by the results of NH_3, NO and O_2 co-adsorption, which enhance the adsorption of ammonia in the form of more thermally stable NH_4^+ than NH_3(ads) on Lewis acid sites [4,45], and thus effectively inhibit the deep oxidation of ammonia. In this way, WO_x-ZrO_2 as support provides moderate Lewis acidity and abundant Brønsted acidity to balance the activity of catalysts for NH_3-SCR and ammonia oxidation. As a result, the $Cu10W10ZrO_2$ catalyst presents the highest NH_3-SCR activity and widest temperature window. However, the more detailed mechanism still needs to be investigated.

It is found that the selectivity to N_2 for NH_3-SCR reaction decreases with the loading amount of copper oxide and increases with tungsten modification, which is also related to the acid property of the catalyst. According to the results of XRD, XPS and NH_3 chemisorption, the formation of WO_x–ZrO_2 solid solutions results in lower-valent copper species and consequently decreases the Lewis acidity [35–40]. Thus, the ammonia oxidation ability of tungsten-containing catalysts is reduced compared to $Cu10ZrO_2$. Ammonia oxidation at high temperature leads to the NH_3 shortage in reactant gases and oxidation of NO to NO_2 in excess O_2. Consequently, NO_2 production correlates well with the loading amount of CuO_x (Eq. (11)).

N_2O is known to be mainly produced through ammonia nitrate decomposition or ammonia oxidation over CuO_x-containing catalysts [29,48] (Eqs. (17)–(20)). In this work, both nitrate formation and ammonia oxidation are restrained by WO_x modification due to decreased Lewis acidity and increased Brønsted acidity (which may arise from the partially hydrated tungsten species [45]) with lower oxidation activity. Therefore, N_2O generation amount is greatly reduced on CuO_x/WO_x–ZrO_2 and is close to zero on WO_x–ZrO_2

$$NO_2(ads) + O(ads) \rightarrow NO_3^-(ads) \quad (17)$$

$$NH_4^+(ads) + NO_3^-(ads) \rightarrow NH_4NO_3(ads) \quad (18)$$

$$NH_4NO_3(ads) \rightarrow N)_2O + 2H_2O \quad (19)$$

$$2HNO(ads) \rightarrow H_2O + N_2O \quad (20)$$

5. Conclusions

$CuO_x/WO_x–ZrO_2$ catalysts were prepared via two steps, and their activities for ammonia oxidation and NH_3-SCR were evaluated. 10 wt.% $CuO_x/WO_x–ZrO_2$ catalyst shows remarkably enhanced NH_3-SCR performances than WO_x-ZrO_2 and $CuO_x–ZrO_2$ catalysts, achieving NO conversion exceeding 80% at a wide temperature range (200–320 °C). The onset temperatures of NH_3-TPO and NH_3-SCR on catalysts depend on acid properties introduced by CuO_x and $WO_x–ZrO_2$ support. Two different reaction routes, "ammonia–NO_2 route" at low temperatures (<200 °C) and "amine–NO/NO_2" at high temperatures (>250 °C), are presented based on the experimental results. In such mechanisms, $WO_x–ZrO_2$ as support provides moderate Lewis acidity and abundant Brønsted acidity to balance the activity of $CuO_x/WO_x–ZrO_2$ for NH_3-SCR and ammonia oxidation. And the Lewis acid sites introduced by copper oxide result in easier formation of nitro compounds and the quick adsorption/desorption of NO/NO_2 on catalysts, facilitating the higher NH_3-SCR activity.

Acknowledgments

The authors would like to acknowledge the Ministry of Science and Technology, PR China for the financial support of Project 2009AA064801 and 2010CB732304. Moreover, we would also like to thank the Ministry of Industry and Information Technology, PR China and State Key Lab of New Ceramics and Fine Processing in Tsinghua University.

References

[1] G. Busca, M.A. Larrubia, L.A.G. Ramis, Catal. Today 107–108 (2005) 139.
[2] J. Hao, L. Wang, M. Shen, L. Li, J. Hu, Environ. Pollut. 147 (2007) 401.
[3] C.K. Chan, X. Yao, Atmos. Environ. 42 (2008) 1.
[4] G. Busca, L. Lietti, G. Ramis, F. Berti, Appl. Catal. B 18 (1998) 1.
[5] R. Burch, J.P. Breen, F.C. Meunier, Appl. Catal. 39 (2002) 283.
[6] L. Lietti, I. Nova, P. Forzatti, J. Catal. 257 (2008) 270.
[7] J. Kašpar, P. Fornasiero, Neal Hickey, Catal. Today 77 (2003) 419.
[8] L. Lietti, G. Ramis, F. Berti, G. Toledo, D. Robba, G. Busca, P. Forzatti, Catal. Today 42 (1998) 101.
[9] I. Nova, C. Ciardelli, E. Tronconi, D. Chatterjee, B. Bandl-Konrad, Catal. Today 114 (2006) 3.
[10] L. Xu, R.W. McCabe, R.H. Hammerle, Appl. Catal. B 39 (2002) 51.
[11] M.V. Twigg, Appl. Catal. B 70 (2007) 2.
[12] M. Kang, D.J. Kim, E.D. Park, J.M. Kim, J.E. Yie, S.H. Kim, L. Hope-Weeks, E.M. Eyring, Appl. Catal. B 68 (2006) 21.
[13] M. Brandhorst, J. Zajac, D.J. Jones, J. Rozière, M. Womes, A. Jimenez-López, E. Rodríguez-Castellón, Appl. Catal. B 55 (2005) 267.
[14] Z. Wu, B. Jiang, Y. Liu, Appl. Catal. B 79 (2008) 347.
[15] A.D. Paola, E. García-López, G. Marcì, C. Martìn, L. Palmisano, V. Rives, A.M. Venezia, Appl. Catal. B 76 (2007) 123.
[16] H.H. Phil, M.P. Reddy, P.A. Kumar, L.K.S. Hyo, Appl. Catal. B 78 (2008) 301.
[17] M. Devadas, O. Kröcher, M. Elsener, A. Wokaun, N. Söger, M. Pfeifer, Y. Demel, L. Mussmann, Appl. Catal. B 67 (2006) 187.
[18] A. Sultana, M. Haneda, T. Fujitani, H. Hamada, Micropor. Mesopor. Mater. 111 (2008) 488.
[19] R. Moreno-Tost, J. Santamaría-González, E. Rodríguez-Castellón, A. Jiménez-López, Appl. Catal. B 52 (2004) 241.
[20] S. Dzwigaj, J. Janas, W. Rojek, L. Stievano, F.E. Wagner, F. Averseng, M. Che, Appl. Catal. B 86 (2009) 45.
[21] Y. Cheng, J. Hoard, C. Lambert, J.H. Kwak, C.H.F. Peden, Catal. Today 136 (2008) 34.
[22] J.H. Park, H.J. Park, J.H. Baik, I.S. Nam, C.H. Shin, J.H. Lee, B.K. Cho, S.H. Oh, J. Catal. 240 (2006) 47.
[23] M. Richter, R. Eckelt, B. Parlitz, R. Fricke, Appl. Catal. B 15 (1998) 129.
[24] T. Venkov, M. Dimitrov, K. Hadjiivanov, J. Mol. Catal. A 243 (2006) 8.
[25] D. Pietrogiacomi, D. Sannino, A. Magliano, P. Ciambelli, S. Tuti, V. Indovina, Appl. Catal. B 36 (2002) 217.
[26] A. Caballero, J.J. Morales, A.M. Cordon, J.P. Holgado, J.P. Espinos, A.R. Gonzalez-Elipe, J. Catal. 235 (2005) 295.
[27] D. Pietrogiacomi, A. Magliano, D. Sannino, M.C. Campa, P. Ciambelli, V. Indovina, Appl. Catal. B 60 (2005) 83.
[28] G. Delahay, B. Coq, E. Ensuque, F. Figuéras, Langmuir 13 (1997) 5588.
[29] S. Suárez, J.A. Martín, M. Yates, P. Avila, J. Blanco, J. Catal. 229 (2005) 227.
[30] J.A. Sullivan, J.A. Doherty, Appl. Catal. B 55 (2005) 185.
[31] X. Jiang, G. Ding, L. Lou, Y. Chen, X. Zheng, J. Mol. Catal. A 218 (2004) 187.
[32] G. Ramis, L. Yi, G. Busca, M. Turco, E. Kotur, R.J. Willey, J. Catal. 157 (1995) 523.
[33] G. Centi, S. Perathoner, Appl. Catal. A 132 (1995) 179.
[34] J.P. Chen, R.T. Yang, Appl. Catal. A 80 (1992) 135.
[35] J.R. Sohn, M.Y. Park, Langmuir 14 (1998) 6140.
[36] T. Onfroy, G. Clet, M. Houalla, J. Phys. Chem. B 109 (2005) 3345.
[37] M.A. Cortés-Jácome, C. Angeles-Chavez, X. Bokhimi, J.A. Toledo-Antonio, J. Solid State Chem. 179 (2006) 2663.
[38] A. Martínez, G. Prieto, M.A. Arribas, P. Concepción, J.F. Sánchez-Royo, J. Catal. 248 (2007) 288.
[39] J.S. da Cruz, M.A. Fraga, S. Braun, L.G. Appel, Appl. Surf. Sci. 253 (2007) 3160.
[40] F.D. Gregorio, V. Keller, J. Catal. 225 (2004) 45.
[41] J. Due-Hansen, A.L. Kustov, S.B. Rasmussen, R. Fehrmann, C.H. Christensen, Appl. Catal. B 66 (2006) 161.
[42] K.I. Hadjiivanov, Catal. Rev. 42 (2000) 71.
[43] L. Zhang, H. He, J. Catal. 268 (2009) 18–25.
[44] J.A. Sullivan, J.A. Doherty, Appl. Catal. B 55 (2005) 185–194.
[45] J. Due-Hansen, A.L. Kustov, C.H. Christensen, R. Fehrmann, Catal. Commun. 10 (2009) 803.
[46] A. Gutirrez-Alejandre, J. Ramrez, G. Busca, Langmuir 14 (1998) 630.
[47] I. Nova, L. Lietti, E. Tronconi, P. Forzatti, Catal. Today 60 (2000) 73.
[48] G. Centi, S. Perathoner, D. Biglino, E. Giamello, J. Catal. 151 (1995) 75.